Acetylcholinesterase active centre and gorge conformations analysed by combinatorial mutations and enantiomeric phosphonates

Zrinka KOVARIK*†[1], Zoran RADIĆ*, Harvey A. BERMAN‡, Vera SIMEON-RUDOLF†, Elsa REINER† and Palmer TAYLOR*

*Department of Pharmacology, University of California at San Diego, La Jolla, CA 92093-0636, U.S.A., †Institute for Medical Research and Occupational Health, Ksaverska cesta 2, POB 291, HR-10000 Zagreb, Croatia, and ‡Department of Pharmacology and Toxicology, School of Medicine, University at Buffalo, Buffalo, NY 14214, U.S.A.

A series of eight double and triple mutants of mouse acetylcholinesterase (AChE; EC 3.1.1.7), with substitutions corresponding to residues found largely within the butyrylcholinesterase (BChE; EC 3.1.1.8) active-centre gorge, was analysed to compare steady-state kinetic constants for substrate turnover and inhibition parameters for enantiomeric methylphosphonate esters. The mutations combined substitutions in the acyl pocket (Phe^{295} →Leu and Phe^{297} → Ile) with the choline-binding site (Tyr^{337} → Ala and Phe^{338} → Ala) and with a side chain (Glu^{202} → Gln) N-terminal to the active-site serine, Ser^{203}. The mutations affected catalysis by increasing K_m and decreasing k_{cat}, but these constants were typically affected by an order of magnitude or less, a relatively small change compared with the catalytic potential of AChE. To analyse the constraints on stereoselective phosphonylation, the mutant enzymes were reacted with a congeneric series of S_P- and R_P-methylphosphonates of known absolute stereochemistry. Where possible, the overall reaction rates were deconstructed into the primary constants for formation of the reversible complex and intrinsic phosphonylation. The multiple mutations greatly reduced the reaction rates of the more reactive S_P-methylphosphonates, whereas the rates of reaction with the R_P-methylphosphonates were markedly enhanced. With the phosphonates of larger steric bulk, the enhancement of rates for the R_P enantiomers, coupled with the reduction of the S_P enantiomers, was sufficient to invert markedly the enantiomeric preference. The sequence of mutations to enlarge the size of the AChE active-centre gorge, resembling in part the more spacious gorge of BChE, did not show an ordered conversion into BChE reactivity as anticipated for a rigid template. Rather, the individual aromatic residues may mutually interact to confer a distinctive stereospecificity pattern towards organophosphates.

Key words: acetylcholinesterase mutation, butyrylcholinesterase mutation, organophosphate inhibition, stereoselectivity.

INTRODUCTION

Acetylcholinesterase (AChE; EC 3.1.1.7) and butyrylcholinesterase (BChE; EC 3.1.1.8) are serine hydrolases that structurally belong to the class of proteins known as the esterase/lipase family within the α/β-hydrolase-fold superfamily [1]. AChE and BChE display substantial similarity in their structures, yet differ in substrate specificities and sensitivities to a wide range of inhibitors [2–4]. The available three-dimensional structures of AChE coupled with kinetic studies of the AChE mutants with substrates and inhibitors delineate domains within the active site [3,5,6]. Besides the catalytic triad Ser^{203}-His^{447}-Glu^{334}, the active site includes the oxyanion hole consisting of Gly^{121}, Gly^{122} and Ala^{204}, the choline binding site Trp^{86}, Tyr^{337}, Phe^{338}, and the acyl pocket Phe^{295} and Phe^{297} (throughout the present paper, numbers refer to the numbering of amino acid residues in mouse AChE). In BChE, which, unlike AChE, can efficiently catalyse hydrolysis of larger molecules such as butyrylcholine and benzoylcholine, modified substrate selectivity was shown to result mainly from differences in the acyl-pocket structure between the two enzymes [3,5,7]. Aliphatic residues of smaller dimensions are found at positions corresponding to Leu^{295} and Ile^{297} in BChE allowing larger substrates to fit into the active site in an orientation appropriate for efficient catalysis [1,8]. Cholinesterases also catalyse phosphonylation of the catalytic serine by organophosphonates. However, unlike carboxyl ester substrates, the phosphonylated enzyme reacts slowly with water,

rendering long-lasting conjugation and inhibition of the enzyme. Furthermore, the AChE reaction with organophosphates displays marked stereoselectivity that can also be utilized for investigation of the steric interactions with structural elements of the active centre [9–12]. The tetrahedral organophosphates contain substituents on the phosphorus atom with ideal bond angles of 109°. Therefore their substituent groups will project differently in the active site from those in planar substrates with trigonal, ideally 120°, bond angles. In the case of the organophosphate–AChE interaction the three-point attachment comes from (i) a conjugating bond distance between the active site serine and the phosphonyl phosphorus, (ii) entry of the phosphonyl oxygen into the oxyanion hole, and (iii) the thiocholine leaving group directed towards the gorge exit [13].

Because the cholinesterases contain the inherent power of stereoselectivity, and because their interaction with organophosphates enables one to deconstruct steady-state catalysis, in order to examine the transesterification step directly, we have examined the influence of multiple site-directed mutations in AChE on substrate turnover and active-centre serine phosphonylation. Mutants were subjected to phosphonylation by a series of enantiomeric pairs, S_P and R_P, of alkyl methylphosphonates in which the structure of the alkoxy group was varied: isopropyl, 3,3-dimethylbutyl and cycloheptyl methylphosphonyl thiocholine (iPrMPTCh, DMBMPTCh and CHMPTCh respectively; Figure 1). Double and triple mutants of mouse AChE with residue substitutions at selected positions
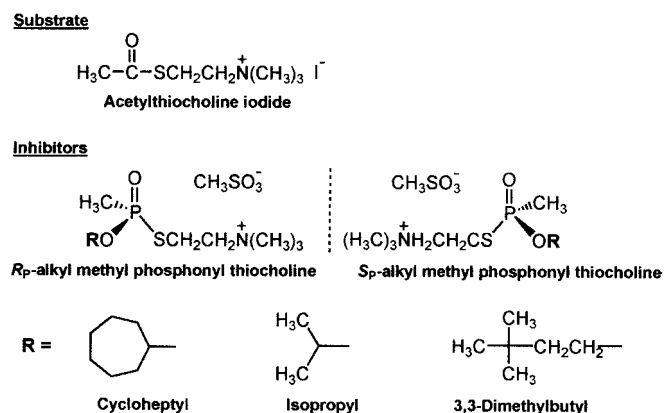
Figure 1   Structures of the substrate and inhibitors employed in the present study

in the active-centre gorge (Figure 2) were prepared to correlate, through structural perturbations, the functional architecture of the AChE gorge with the reactivity and stereoselectivity of the chiral phosphonates. Catalytic constants for acetylthiocholine iodide (ATCh) hydrolysis and rates of phosphonylation of mutant enzymes were evaluated with respect to the structure and steric orientation of the substrate and selected amino acid residues within the active-centre gorge of the enzyme. Multiple mutants of AChE containing F295L (Phe[295] → Leu), F297I and Y337A have enabled us to dissect the structural basis for the divergence between AChE and BChE inhibitor specificity and kinetics.

MATERIALS AND METHODS

Chemicals

S_P- and R_P-alkyl methylphosphonyl thiocholines (Figure 1) were synthesized and isolated as resolved S_P and R_P enantiomers [9]. Stock solutions in acetonitrile were kept at $-20\,°C$, and aliquots were diluted in water immediately before use. MEPQ [7-(methylethoxyphosphinyloxy)-1-methylquinolinium iodide] and DEPQ [7-(O,O-diethylphosphinyloxy)-1-methylquinolinium methyl sulphate] prepared by Dr H. Leader and Dr Y. Ashani (Israel Institute for Biological Research, Ness Ziona, Israel) were gifts from Dr B. P. Doctor (Walter Reed Army Research Center, Washington, DC, U.S.A.). MEPQ dissolved in acetone and DEPQ dissolved in acetonitrile were kept at $-20\,°C$. ATCh, DTNB [5,5′-dithiobis-(2-nitrobenzoic acid)] and BSA were purchased from Sigma Chemical Co., St. Louis, MO, U.S.A.

Production and purification of AChE

Preparation of the cDNA that encodes mouse AChE truncated at position 548, which yields a monomeric form of the enzyme, has been described previously in [14] and was used in mutagenesis as the template wild-type cDNA. Mutant mouse AChE cDNAs were generated by PCR-mediated standard mutagenesis procedures (QuikChange® Kit; Stratagene, San Diego, CA, U.S.A.). Multiple mutants were generated by combined subcloning of DNA fragments containing single mutations, or by performing mutagenesis using mutant DNA templates. Finally, cassettes of mutant constructs were subcloned into the mammalian expression vector, pCDNA3 (Invitrogen, San Diego, CA, U.S.A.). The nucleotide sequences of the cassettes were confirmed by double-stranded sequencing.

Transfection of HEK-293 cells (purchased from American Type Culture Collection, Atlanta, GA, U.S.A.), as well as selection of expressing cells by aminoglycoside resistance conferred by co-transfection of a neomycin acetyltransferase gene, were described previously in [10]. Stable transfectants were grown to confluence in either 10-cm-diameter dishes or three-tiered flasks with a cell growth surface area of $500\,cm^2$ (Nalge Nunc International, Rochester, NY, U.S.A.) before replacement of the foetal-bovine-serum-supplemented Dulbecco's modified Eagle's medium with serum-free medium, Ultraculture cell culture medium (BioWhittaker, Walkersville, MD, U.S.A.). Harvests of the medium containing the soluble monomeric form of AChE were performed at 2–3 day intervals; by replacement of medium on the cell monolayers, cultures could be continued for several weeks.

Several litres of media were subjected to affinity chromatography to purify the mutant enzymes, typically in amounts of 2–10 mg. Procainamide affinity resin utilized CNBr-activated Sepharose CL-4B resin with a hexanoic alkyl chain [15]. Harvested ultraculture medium containing the expressed enzyme was centrifuged (2000 g for 15 min at 4 °C), and was assayed for AChE activity. MgCl$_2$ was added to a final concentration of 40 mM, then the resin suspension (1 ml for each 2 mg of AChE) and the mixture were allowed to stir in a spinner flask (Bellco, Wineland, NJ, U.S.A.) overnight at 4 °C in the presence of 0.02 % (w/v) NaN$_3$. The medium was poured into a Bio-Rad Econo-column (Bio-Rad, Hercules, CA, U.S.A.), was allowed to pack by sedimentation, and then washed with equilibrating buffer [at 50–100 times the bed volume; 10 mM NaHCO$_3$, 100 mM NaCl, 40 mM MgCl$_2$ and 0.02 % (w/v) NaN$_3$, pH 8]. The enzyme was subsequently eluted by competition with 100 mM decamethonium bromide, at a low flow rate ($1–1.5\,ml \cdot h^{-1}$). The purified enzyme was dialysed using the 14–16 kDa cut-off dialysis tubing (Spectrapore, Houston, TX, U.S.A.) against 4 litres of dialysis buffer [10 mM Tris/HCl, 100 mM NaCl, 40 mM MgCl$_2$ and 0.02 % (w/v) NaN$_3$, pH 8.0] four times for 6 h. Pools of purified enzyme were stored at 4 °C.

AChE activity measurements

Enzyme activities were determined at 22 °C by the Ellman method using ATCh as substrate [16]. Reactions were started by adding substrate to 100 mM phosphate buffer, pH 7.0, containing 0.01 % (v/v) BSA, 0.33 mM DTNB and enzyme. The linear increase of absorbance was monitored from 15 s to 2 min against a blank containing buffer, BSA and DTNB. Maximum concentrations of ATCh did not exceed 100 mM. Whenever ATCh concentrations were greater than 1.0 mM, enzyme activity was corrected for spontaneous non-enzymic substrate hydrolysis.

Known concentrations of MEPQ or DEPQ were utilized to titrate the number of active sites, according to procedures described previously in [17,18].

AChE inhibition by organophosphates

In the inhibition experiments, enzyme samples were incubated for > 30 min with organophosphonates [in 100 mM phosphate buffer, pH 7.0, containing 0.01 % (v/v) BSA] in the absence of substrate; typically, three to five inhibitor concentrations were used. The inhibition reaction was stopped by the addition of ATCh (1.0 mM final concentration), and the extent of inhibition was determined by measuring the residual activity. To obtain the enzymic activity at time-zero inhibition, the enzyme was added to the reaction medium containing inhibitor and substrate.
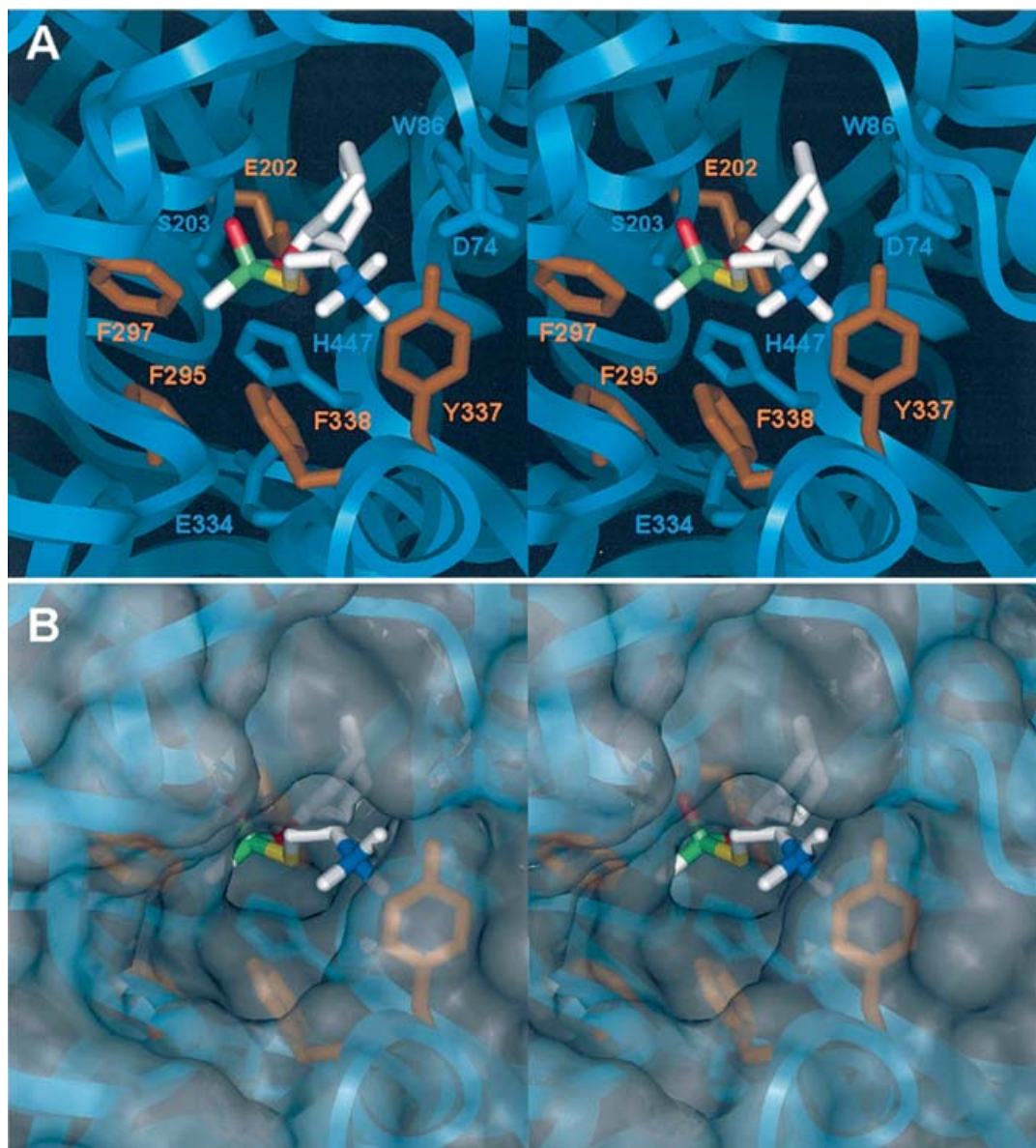
Figure 2   Stereo image of S_P-CHMPTCh bound in the active centre of wild-type mouse AChE in the form of a Michaelis-type complex (cf. Scheme 2)

The image is based on computational analysis of the organophosphate binding in the AChE active centre described previously by Hosea et al. [21]. (**A**) The organophosphate is represented by white (carbon), red (oxygen), blue (nitrogen) and green (phosphorus) sticks. The five AChE side chains where mutations were made are represented by orange sticks, while the catalytic triad residues (Ser[203], Glu[334] and His[447]) are coloured blue. Two additional AChE residues important for interaction with ligands, Trp[86] and Asp[74], are also displayed. The protein α-carbon backbone of mouse AChE (taken from Protein Data Bank entry 1maa) is displayed as a blue ribbon. (**B**) Transparent, solvent-accessible Connolly AChE surface, for the complex shown in (**A**). The shape of the surface illustrates spatial restrictions in the enzyme active-centre gorge imposed by the mutated and neighbouring residues.

Kinetic equations

The evaluation of catalytic parameters was based on Scheme 1 (compare with [19]). According to this scheme, the enzyme (E) associates reversibly with substrate (S) forming two binary complexes: the ES complex in the active site and the SE complex in a secondary peripheral site. The complex ES results in substrate hydrolysis with the rate constant k_{cat}, whereas the SE complex is inactive. The ternary complex SES leads to substrate hydrolysis with a rate constant $b\,k_{cat}$. Scheme 1 assumes that S has equal affinity for the active site of E and SE as does S for a peripheral site of E and ES. Constants K_s and K_{ss} are the respective ES and SE dissociation constants. The K_s constant approximates to the Michaelis constant K_m. Throughout the present paper the symbol

K_m will therefore be used instead of K_s. Eqn (1) describes catalysis in Scheme 1:

$$v_0 = \frac{e_0 \cdot k_{cat}}{1 + \dfrac{K_m}{[S]}} \cdot \frac{1 + b\dfrac{[S]}{K_{SS}}}{1 + \dfrac{[S]}{K_{SS}}} \tag{1}$$

where v_0 is the initial steady-state rate of ATCh hydrolysis and e_0 is the total enzyme active-site concentration. The catalytic parameters were calculated by fitting experimental data to eqn (1) [3,19].

Scheme 1   Reaction scheme for substrate hydrolysis by acetylcholinesterase

Modified from [19].

Scheme 2   Progressive inhibition of acetylcholinesterase by organophosphates

Modified from [20].

Progressive inhibition of AChE by organophosphates is defined by Scheme 2 (cf. [20]). Enzyme (E) and organophosphate (OP) form a reversible Michaelis-type complex ([E][OP]) from where the covalently phosphorylated enzyme (EP) and the leaving group of the organophosphate arise; k_{+2} is the first-order inhibition rate constant and k_i is the overall second-order rate constant of inhibition. Scheme 2 is defined by eqn (2):

$$\ln \frac{v_0}{v_i} = \frac{k_{+2} \cdot [OP]}{K_i + [OP]} \cdot t = k_{obs} \cdot t \tag{2}$$

where v_0 and v_i stand for the enzyme activity in the absence and in the presence of inhibitor (OP) respectively at the time of inhibition (t). K_i approximates to the dissociation constant of the [E][OP] complex, and k_{obs} is the first-order rate constant of inhibition determined at any given inhibitor concentration. The k_{+2} and K_i constants were calculated from eqn (2).

When $[OP] \ll K_i$, constants k_{+2} and K_i cannot be separately evaluated, because eqn (2) reduces to eqn (3):

$$\ln \frac{v_0}{v_i} = \frac{k_{+2}}{K_i} \cdot [OP] \cdot t = k_i \cdot [OP] \cdot t = k_{obs} \cdot t \tag{3}$$

from which k_i was calculated. The k_i constant corresponds to the ratio k_{+2}/K_i.

RESULTS AND DISCUSSION

Effect of mutations on catalytic constants of ATCh hydrolysis

All multiple AChE mutants contain mutations inside the active-centre gorge of mouse AChE, and many resemble the residue replacements in the mouse BChE active site (F295L, F297I and Y337A). The activity of the enzymes for ATCh is shown in Figure 3. The bell-shaped pS-curve of wild-type AChE activity reached an optimum at about 1 mM ATCh. Only the mutants, F295L/Y337A and F295L/Y337A/F338A, exhibited bell-shaped pS-curves similar to that of wild-type AChE, but reached a

Figure 3   Concentration dependencies of ATCh hydrolysis by wild-type and mutant AChEs

Activities are expressed in moles of hydrolysed substrate per mole of enzyme active sites per minute. The curves were generated using eqn (1). (**A**) Wild-type AChE (●) and mutants with mutations progressing from AChE to BChE: F295L/Y337A (■), F297I/Y337A (▲) and F295L/F297I/Y337A (▽). (**B**) Wild-type AChE (- - - -) and mutants with E202Q and F338A substitutions: Y337A/F338A (▽), F295L/Y337A/F338A (●) and E202Q/F295L/Y337A (□). (**C**) Wild-type AChE (- - - -) and mutants with alanine substitutions: F295A/Y337A (▲) and F295A/F297A/Y337A (□).

maximum at higher ATCh concentrations, whereas pS-curves of the other mutants resembled that of BChE [21–23].

All mutations studied revealed an increase of K_m and a decrease of k_{cat} compared with AChE (Table 1). Two mutants, F295L/Y337A and Y337A/F338A, had a k_{cat} similar to that of BChE. As a result of both a higher K_m and lower k_{cat}, the efficiency of catalysis (k_{cat}/K_m) of the mutants at low substrate concentrations is less than that of wild-type AChE. Alanine at positions 295 and 297 resulted in a reduction of k_{cat}, and compared with the corresponding mutants F295L/Y337A and F295L/F297I/Y337A, alanine substitution led to a further reduction in catalytic constants (cf. Table 1). In contrast, the single mutants, F295A and F297A, showed greater catalytic rates than the F295L and F297I mutants [10]. This combinatorial behaviour might be a consequence of altered structural integrity of the acyl pocket in the mutant enzyme. Replacement of the large phenylalanine residue with alanine can be expected to yield a void area, which should be

Table 1   Catalytic constants for ATCh catalysis by recombinant DNA-derived mouse cholinesterases

Constants were obtained by non-linear regression analysis of data from pS-curves according to Scheme 1 and eqn (1). Results are means $\pm$ S.D. ($n = 3$–5).

Enzyme	K_m (μM)	K_{ss} (mM)	b	k_{cat} (10^4 min^{-1})	k_{cat}/K_m (10^7 min$^{-1} \cdot$ M^{-1})
AChE wild-type	47 ± 7	9.6 ± 2.0	0.20 ± 0.04	15 ± 4	320
BChE wild-type*	35 ± 2	1.3 ± 0.5	3.6 ± 0.2	4.0 ± 0.7	110
F295L/Y337A	100 ± 7	62 ± 30	0.62 ± 0.07	4.0 ± 0.2	40
F297I/Y337A	340 ± 100	5.5 ± 3.4	5.7 ± 2.1	1.4 ± 0.4	4.1
F295A/Y337A	76 ± 20	2.4 ± 0.2	3.3 ± 0.6	2.0 ± 0.2	26
Y337A/F338A	150 ± 80	14 ± 8	2.6 ± 0.9	3.9 ± 0.5	26
F295L/F297I/Y337A	69 ± 30	21 ± 19	3.2 ± 0.5	1.5 ± 0.5	22
F295A/F297A/Y337A†	190	9.1	3.6	1.1	5.8
F295L/Y337A/F338A	150 ± 20	14 ± 7	0.33 ± 0.07	1.7 ± 0.1	11
E202Q/F295L/Y337A	100 ± 40	38 ± 10	7.1 ± 5.3	1.0 ± 0.1	10

* Radić et al. [3].
† One experiment only.

occupied with water or result in collapse of the α-carbon chain. For the F295L and F297I substitutions, the volume reduction and structural perturbation is smaller and less impacted by the concomitant Y337A substitution on the opposite face of the gorge. The aromatic residues F295, F297 and Y337 may serve to stabilize and orient ATCh for efficient catalysis. It should be noted that no natural cholinesterase identified at the present time contains alanine at positions corresponding to 295 and 297 in mouse AChE [1,24].

Inhibition by excess substrate, resulting in bell-shaped pS-curves, is explained by the binding of a substrate molecule to the peripheral site of the enzyme [19,25]. Residues in the acyl pocket and choline-binding site do influence K_{ss} and b values, demonstrating that these residues are linked to the catalytic influence of the binding of a second substrate molecule. The F295L substitution in the Y337A mutant shows a catalytic profile that resembles AChE in that this double mutant displays substrate inhibition ($b < 1$), whereas the F297I substitution in Y337A resembles BChE, where the double mutant shows apparent substrate activation ($b > 1$). The single mutants F295L and F297I show similar changes in the b parameter to those of the double mutant [3,10], showing that the Y337A substitution is not involved in the inhibition/activation process. Substitution F295L in the triple mutant F295L/Y337A/F338A also prevents the apparent substrate activation seen in Y337A/F338A (Figure 3). On the other hand, comparison of catalytic parameters of F295L/Y337A and E202Q/F295L/Y337A gives rise to the conclusion that the E202Q mutation is responsible for the apparent substrate activation ($b > 1$, cf. Table 1). Previous results showed that the single mutation E202Q of mouse AChE only slightly altered K_m and k_{cat}, but changed the K_{ss} and b values [21], and that the charge on Glu^{202} probably has a role in stabilization of the transition state [26–28].

Conformational changes of the acyl-pocket loop following conjugation of a large organophosphate and aging of the conjugate were reported in crystal-structure analysis of *Torpedo californica* AChE [29]. It is therefore reasonable to assume that mutations of phenylalanine residues to isoleucine, leucine or alanine could affect flexibility of the loop that encompasses peripheral site residues and may link the active site with the peripheral site. The concept of a functional linkage was first suggested by Changeux [30] to explain allosteric binding of certain inhibitors to AChE; later it was demonstrated directly with fluorescence spectra of ligands bound at the peripheral site or active centre [31,32].

Table 2   Constants ($\pm$ S.E.M.) for inhibition of recombinant-DNA-derived mouse cholinesterases by chiral thiocholine methylphosphonates

The first-order inhibition constant (k_{+2}) and enzyme–inhibitor equilibrium dissociation constant (K_i) were determined by non-linear regression of eqn (2) from k_{obs} constants (9–14 values) obtained from at least three experiments.

Enzyme	Inhibitor	k_{+2} (min^{-1})	K_i (nM)	k_i (10^6 min$^{-1} \cdot$ M^{-1})
F297I/Y337A	R_P-iPrMPTCh	0.6 ± 0.2	220 ± 130	2.8 ± 1.8
F295L/F297I/Y337A	S_P-CHMPTCh	1.1 ± 0.3	36 ± 15	32 ± 17
F295L/F297I/Y337A	R_P-CHMPTCh	0.6 ± 0.2	74 ± 49	8.1 ± 6.0
F295L/Y337A/F338A	S_P-CHMPTCh	1.3 ± 0.4	83 ± 49	16 ± 11
E202Q/F295L/Y337A	S_P-DMBMPTCh	3.8 ± 1.1	12 ± 5	330 ± 180

With the exception of F295L/Y337A/F338A, all other AChE mutants retained substantial catalytic capacity irrespective of whether their pS-profiles mimicked that of AChE or BChE.

Mutation analysis and phosphonylation of AChE

Mouse cholinesterases were phosphonylated by S_P and R_P enantiomers of CHMPTCh, iPrMPTCh or DMBMPTCh (Figure 1). The phosphonate concentration was in excess of the enzyme concentration, and the inhibition followed first-order kinetics. The constants k_{+2}, K_i and k_i were evaluated from the dependence of k_{obs} on the concentration of inhibitor [cf. eqns (2) and (3)]. Three different patterns for inhibition kinetics were obtained, as shown in Figures 4(A)–4(C). For most reactions (32 out of 43) a linear dependence of k_{obs} on the phosphonate concentration was obtained (Figure 4A), which did not allow the distinction of individual constants k_{+2} and K_i. The same applies to the reactions (6 out of 43) presented in Figure 4(B). The y-axis intercepts in Figures 4(B) and 4(C) are probably due to the formation of a reversible enzyme–inhibitor complex in which the inhibitor was not fully displaced by 1 mM ATCh that was used in the activity assay. This initial complex was not studied further. In Figure 4(C), a non-linear dependence of k_{obs} on the inhibitor concentration enabled us to calculate the primary constants for formation of the reversible complex (K_i) and the intrinsic phosphonylation constant (k_{+2}) using eqn 2 (Table 2). The k_{+2} values for R_P compounds were typically less than one-half of k_{+2} for the S_P compounds, whereas K_i ranged between 12 and
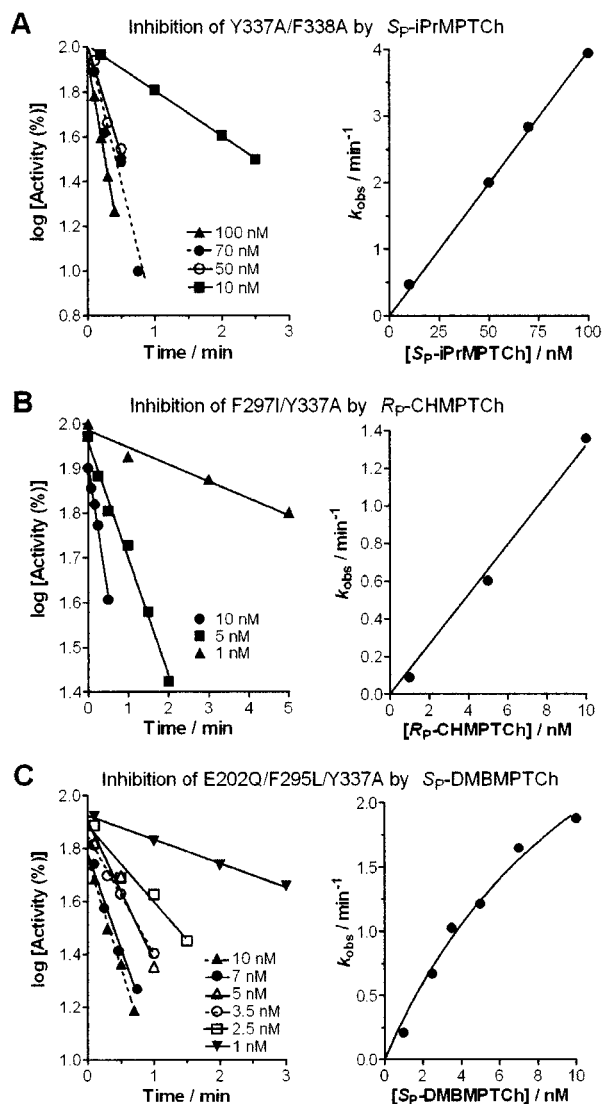
Figure 4   Representative inhibition experiments of AChE mutants by alkyl methylphosphonyl thiocholines

From the analysis of inhibition at zero time (i.e. intercept on the y-axis), and from the relationship between k_{obs} and inhibitor concentrations, inhibition kinetics displayed three different patterns: (**A**) all inhibition lines pass through log[Activity (%)] = 2.0, and k_{obs} was linearly dependent on inhibitor concentration; (**B**) the y-intercept is below 100 % activity, whereas k_{obs} and inhibitor concentration still show a linear relationship; (**C**) the inhibition lines also intercept the y-axes below 100 % activity, but k_{obs} against inhibitor concentration deviates from linearity and approaches a limiting value at high inhibitor concentrations. This indicates that an appreciable concentration of enzyme–inhibitor complex is accumulating.

Table 3   Rate constants (k_i) for the inhibition of recombinant-DNA-derived mouse cholinesterases by S_P- and R_P-CHMPTCh enantiomers

Eqn (3) was applied to calculate k_i ($\pm$ S.E.M.) from k_{obs} constants (6–10 values) obtained from at least three experiments.

Enzyme	k_i (10^6 min$^{-1} \cdot$ M^{-1})		$k_i(S_P)/k_i(R_P)$
	S_P	R_P	
AChE wild-type*	190 ± 30	0.81 ± 0.09	230
F295L*	66 ± 9	8.7 ± 1.1	7.6
F297I*	16 ± 3	62 ± 3	0.26
Y337A†	120 ± 10	0.84 ± 0.04	140
E202Q†	21 ± 2	0.13 ± 0.01	160
F295L/Y337A	140 ± 5	25 ± 2	5.6
F297I/Y337A	8.1 ± 0.7	130 ± 6	0.062
Y337A/F338A	160 ± 4	2.0 ± 0.2	80
F295L/F297I/Y337A	32 ± 17‡	8.1 ± 6.0‡	4.0
F295L/Y337A/F338A	16 ± 11‡	4.5 ± 0.4	3.6
E202Q/F295L/Y337A	64 ± 2	19 ± 1	3.4
BChE wild-type*	470 ± 90	6.7 ± 0.7	70

* [10].
† [21].
‡ From Table 2.

Table 4   Rate constants (k_i) for the inhibition of recombinant DNA-derived mouse cholinesterases by S_P- and R_P-iPrMPTCh enantiomers

Eqn (3) was applied to calculate k_i ($\pm$ S.E.M.) from k_{obs} constants (7–14 values) obtained from at least three experiments.

Enzyme	k_i (10^6 min$^{-1} \cdot$ M^{-1})		$k_i(S_P)/k_i(R_P)$
	S_P	R_P	
AChE wild-type*	16 ± 1	0.14 ± 0.03	110
F295L*	3.4 ± 0.1	1.2 ± 0.1	2.8
F297I*	0.95 ± 0.46	1.2 ± 0.1	0.79
Y337A†	24 ± 3	0.34 ± 0.04	71
E202Q†	0.49 ± 0.02	0.038 ± 0.002	13
F295L/Y337A	7.3 ± 0.2	1.8 ± 0.3	4.1
F297I/Y337A	0.47 ± 0.01	2.8 ± 1.8‡	0.17
Y337A/F338A	41 ± 1	0.28 ± 0.01	150
F295L/F297I/Y337A	0.48 ± 0.03	0.26 ± 0.03	1.8
F295L/Y337A/F338A	0.40 ± 0.01	0.46 ± 0.04	0.87
E202Q/F295L/Y337A	2.9 ± 0.3	0.68 ± 0.05	4.3
BChE wild-type*	10 ± 1	3.3 ± 0.1	3.0

* [10].
† [21].
‡ From Table 2.

220 nM. A two orders of magnitude range of second-order rate constants (k_i) for the phosphonates is primarily due to variation in K_i, the dissociation constant. Hence, K_i appears to be the major determinant of AChE reactivity toward organophosphates [9,20,33].

The high enantiomeric stereoselectivity of wild-type AChE with a preference for S_P over R_P enantiomers was decreased by mutations in the choline-binding site and acyl pocket (Tables 3–5). Generally, the mutations reduced inhibition rates by S_P enantiomers, whereas inhibition rates by R_P enantiomers were enhanced. The most dramatic change in rates was obtained in the inhibition of F297I/Y337A by R_P-CHMPTCh, where the rate was increased 160-fold compared with the k_i of the wild-type AChE (cf. Table 3). Moreover, the mutant F297I/Y337A was inhibited 16-fold more rapidly by R_P- than S_P-CHMPTCh, showing inverted stereospecificity, greatly exceeding the ratio of rates for the single mutant F297I [10].

S_P- and R_P-DMBMPTCh showed the most rapid inhibition rates of the three enantiomeric phosphonate pairs, whereas the enantiomeric selectivity for this pair with wild-type AChE was the lowest of the three (Table 5). Inhibition rates with both DMBMPTCh enantiomers for all other multiple mutants (except Y337A/F338A) slightly decreased compared with that of wild-type AChE. The 3,3-dimethylbutyl moiety, being a primary

Table 5 Rate constants (k_i) for the inhibition of recombinant DNA-derived mouse cholinesterases by S_P- and R_P-DMBMPTCh enantiomers

Eqn (3) was applied to calculate k_i ($\pm$ S.E.M.) from k_{obs} constants (6–9 values) obtained from at least three experiments.

Enzyme	k_i (10^6 min$^{-1} \cdot$ M^{-1})		$k_i(S_P)/k_i(R_P)$
	S_P	R_P	
AChE wild-type*	360 ± 10	19 ± 9	19
F295L*	140 ± 10	10 ± 5	14
F297I*	56 ± 4	12 ± 4	4.7
Y337A†	750 ± 20	19 ± 1	39
E202Q†	120 ± 10	2.7 ± 0.1	44
F295L/Y337A	220 ± 20	13 ± 1	17
F297I/Y337A	28 ± 2	12 ± 1	2.3
Y337A/F338A	890 ± 120	39 ± 1	22
F295L/F297I/Y337A	32 ± 2	4.6 ± 0.2	7
F295L/Y337A/F338A	160 ± 7	8.3 ± 0.3	19
E202Q/F295L/Y337A	330 ± 180‡	18 ± 1	18
BChE wild-type*	500 ± 150	32 ± 16	16

 * [10].
 † [21].
 ‡ From Table 2.

instead of a secondary alkoxy moiety, has additional degrees of torsional freedom over the cycloheptyl and isopropyl groups. The flexibility conferred from bond rotation, along with the hydrophobicity, may contribute to the greater reactivity of the R_P-DMBMPTCh organophosphate over the other R_P-methylphosphonates. The flexibility of this group may also enhance the S_P reaction through its fit in the choline subsite.

Although the Y337A mutation had a small effect on the rate of phosphonylation, the rate for the Y337A/F338A mutant increased two-fold for all S_P and R_P enantiomers, except for S_P-CHMPTCh, showing a stereoselectivity similar to, or slightly greater than, that of the wild-type AChE (Tables 3–5). Enlargement of the choline-binding site by mutations Y337A and F338A may provide a preferable orientation for organophosphate reactivity in the active centre.

Since the absolute stereochemistry of these phosphonates is known, molecular-dynamics analysis of energy-minimized conformations for S_P- and R_P-methylphosphonates in the active site of mouse AChE revealed the probable arrangement of substituent groups [21,34]. In case of the S_P enantiomer, the methyl-phosphonyl moiety can fit within the space constraints of the acyl pocket, the phosphonyl oxygen enters the oxyanion hole and the leaving group can fit into the space forming the choline subsite, close to the gorge exit (Figure 2). For the R_P enantiomer, placement of the phosphonyl oxygen and the leaving group at these positions confronts a steric constraint of the alkoxy group in the acyl pocket. Alternatively, placement of the methyl group in the acyl pocket requires that either the phosphonyl oxygen is oriented out of the oxyanion hole or the leaving group is directed away from the gorge exit. By enlarging the acyl pocket so that the R_P-alkoxy group orients in that direction, both positioning criteria for efficient phosphonylation can be satisfied and the rates are accelerated. Stabilization of the S_P-methyl group within the confines of the acyl pocket by Phe[295] and Phe[297] (Figure 2) is also critical for efficient reactivity, since rates of phosphonylation by the S_P enantiomers are diminished for the acyl-pocket mutants, especially if Phe[297] is mutated. Furthermore, decreased reactivity of S_P enantiomers, due to replacement of residues at either the

acyl pocket or choline-binding site, is seen in the triple mutant F295L/F297I/Y337A.

Although the F295L/F297I/Y337A mutant resembles mouse BChE in composition of the acyl pocket and choline binding site, its reactivity toward S_P enantiomers is approx. 20-fold lower than that for the mouse wild-type BChE (cf. Tables 3–5). On the other hand, the reactivity of the triple mutant toward R_P enantiomers approached that of BChE, except for R_P-DMBMPTCh, which phosphonylated both AChE and BChE at slower rates. Thus comparison of k_i constants for AChE and BChE with AChE mutants gives rise to the conclusion that the difference between AChE and BChE is not dictated solely by residues in the acyl pocket and the choline-binding site. Despite the 'equivalence' of residues in these regions of the two enzymes, their architectures are different. One difference not inherent in considerations of aromaticity and volume of the active centre is the flexibility of the α-carbon backbone surrounding the acyl pocket. For example, Arg[296] in AChE may be anchored by interactions with Pro[235], Gln[369] and His[405], imparting stability to the pocket, whereas in BChE, the residue at position 296 is serine. The smaller side chain and diminished interactions may be factors in conferring additional flexibility to the BChE acyl pocket. A recent study on a hexa-substituted mutant of human AChE that resembled residues of human BChE showed that this mutant did not mimic the reactivity of human BChE toward substrates and other covalent ligands, and it was suggested that the catalytically productive orientation of the catalytic triad histidine in BChE is maintained by a somewhat different array of interactions than that in AChE [35].

General conclusions

The combinatorial approach to altering the dimensions of the active centre through mutation, when coupled with the greater discriminatory power of a congeneric series of enantiomeric methylphosphonates, reveals several characteristics of the AChE active centre. The overall dimensions of the acyl pocket are the critical determinant in maintaining stereoselectivity. Mutations enlarging the dimensions of the choline subsite, do not, in themselves, reduce stereoselectivity or reactivity. It is only when mutations in the choline subsite are combined with the acyl-pocket mutation at residue 297 that the most dramatic inversion in stereoselectivity is seen. Enhanced reactivity cannot be predicted simply on the basis of the enlarged volume of the gorge, since the favourable characteristics of elimination of steric occlusion may be offset by formation of non-productive complexes in the enlarged gorge. Enlarging the acyl pocket diminishes the reactivity of all of the S_P-methylphosphonates, suggesting that positioning the methyl group within the confines of a small acyl pocket bordered by the two phenylalanine residues optimizes the position of the phosphorus for reaction in AChE. Simple partitioning of volume increases by side-chain removal does not give an ordered increase in reactivity of the R_P compounds.

REFERENCES

1 Cygler, M., Schrag, J. D., Sussman, J. L., Harel, M., Silman, I., Gentry, M. K. and Doctor, B. P. (1993) Relationship between sequence conservation and three-dimensional structure in a large family of esterases, lipases, and related enzymes. Prot. Sci. **2**, 366–382

2 Taylor, P. and Radić, Z. (1994) The cholinesterases: from genes to proteins. Annu. Rev. Pharmacol. Toxicol. **34**, 281–320

3 Radić, Z., Pickering, N. A., Vellom, D. C., Camp, S. and Taylor, P. (1993) Three distinct domains in the cholinesterase molecule confer selectivity for acetylcholinesterase and butyrylcholinesterase inhibitors. Biochemistry **32**, 12074–12084

4 Kovarik, Z., Radić, Z., Grgas, B., Škrinjarić-Špoljar, M., Reiner, E. and Simeon-Rudolf, V. (1999) Amino acid residues involved in the interaction of acetylcholinesterase and butyrylcholinesterase with the carbamates Ro 02-0683 and bambuterol, and with terbutaline. Biochim. Biophys. Acta **1433**, 261–271

5 Ordentlich, A., Barak, D., Kronman, C., Flashner, Y., Leitner, M., Segall, Y., Ariel, N., Cohen, S., Velan, B. and Shafferman, A. (1993) Dissection of the human acetylcholinesterase active center determinants of substrate specificity. Identification of residues constituting the anionic site, the hydrophobic site, and the acyl pocket. J. Biol. Chem. **268**, 17083–17095

6 Bourne, Y., Taylor, P. and Marchot, P. (1995) Acetylcholinesterase inhibition by fasciculin: crystal structure of the complex. Cell **83**, 503–512

7 Vellom, D. C., Radić, Z., Li, Y., Pickering, N. A., Camp, S. and Taylor, P. (1993) Amino acid residues controlling acetylcholinesterase and butyrylcholinesterase specificity. Biochemistry **32**, 12–17

8 Harel, M., Sussman, J. L., Krejci, E., Bon, S., Chanal, P. and Massoulié, J. (1992) Conversion of acetylcholinesterase to butyrylcholinesterase, modeling and mutagenesis. Proc. Natl. Acad. Sci. U.S.A. **89**, 10827–10831

9 Berman, H. A. and Leonard, K. (1989) Chiral reactions of acetylcholinesterase probed with enantiomeric methylphosphonothioates. J. Biol. Chem. **264**, 3942–3950

10 Hosea, N. A., Berman, H. A. and Taylor, P. (1995) Specificity and orientation of trigonal carboxylesters and tetrahedral phosphonylesters in cholinesterase. Biochemistry **34**, 11528–11536

11 Ordentlich, A., Barak, D., Kronman, C., Benschop, H. P., De Jong, L. P. A., Ariel, N., Barak, R., Segall, Y., Velan, B. and Shafferman, A. (1999) Exploring the active center of human acetylcholinesterase with stereomers of an organophosphorus inhibitor with two chiral centers. Biochemistry **38**, 3055–3066

12 Shi, J., Radić, Z. and Taylor, P. (2002) Inhibitors of different structure induce distinguishing conformations in the omega loop, Cys^{69}-Cys^{96}, of mouse acetylcholinesterase. J. Biol. Chem. **277**, 43301–43308

13 Taylor, P., Hosea, N. A., Tsigelny, I., Radić, Z. and Berman, H. A. (1997) Determining ligand orientation and transphosphonylation mechanism on acetylcholinesterase by R_P, S_P enantiomer selectivity and site-specific mutagenesis. Enantiomer **2**, 249–260

14 Marchot, P., Ravelli, R. B. G., Raves, M. L., Bourne, Y., Vellom, D. C., Kanter, J., Camp, S., Sussman, J. L. and Taylor, P. (1996) Soluble monomeric acetylcholinesterase from mouse: expression, purification, and crystallization in complex with fasciculin. Prot. Sci. **5**, 672–679

15 Ralston, J. S., Main, A. R., Kilpatrick, B. F. A. and Chasson, L. (1983) Use of procainamide gels in the purification of human and horse serum cholinesterases. Biochem. J. **211**, 243–250

16 Ellman, G. L., Courtney, K. D., Andres, Jr, V. and Featherstone, R. M. (1961) A new and rapid colorimetric determination of acetylcholinesterase activity. Biochem. Pharmacol. **7**, 88–95

17 Levy, D. and Ashani, Y. (1986) Synthesis and *in vitro* properties of a powerful quaternary methylphosphonate inhibitor of acetylcholinesterase. Biochem. Pharmacol. **35**, 1079–1085

18 Luo, C., Saxena, A., Smith, M., Garcia, G., Radić, Z., Taylor, P. and Doctor, B. P. (1999) Phosphoryl oxime inhibition of acetylcholinesterase during oxime reactivation is prevented by edrophonium. Biochemistry **38**, 9937–9947

19 Webb, J. L. (1963) General principles of inhibition. Enzyme and Metabolic Inhibitors, p. 188, Academic Press, New York

20 Reiner, E. and Radić, Z. (2000) Mechanism of action of cholinesterase inhibitors. In Cholinesterases and Cholinesterase Inhibitors (Giacobini, E., ed.), pp. 103–119, Martin Dunitz, London

21 Hosea, N. A., Radić, Z., Tsigelny, I., Berman, H. A., Quinn, D. M. and Taylor, P. (1996) Aspartate 74 as a primary determinant in acetylcholinesterase governing specificity to cationic organophosphates. Biochemistry **35**, 10995–11004

22 Masson, P., Froment, M.-T., Bartels, C. F. and Lockridge, O. (1996) Asp70 in the peripheral anionic site of human butyrylcholinesterase. Eur. J. Biochem. **235**, 36–48

23 Simeon-Rudolf, V., Reiner, E., Evans, R. T., George, P. M. and Potter, H. C. (1999) Catalytic parameters for the hydrolysis of butyrylthiocholine by human serum butyrylcholinesterase variants. Chem. Biol. Interact. **119–120**, 165–171

24 Cousin, X., Hotelier, T., Giles, K., Lievin, P., Toutant, J.-P. and Chatonnet, A. (1997) ACHEdb: the database system for ESTHER, the α/β fold family of proteins and the cholinesterase gene server. Nucleic Acids Res. **25**, 143–146

25 Aldridge, W. N. and Reiner, E. (1972) Enzyme Inhibitors as Substrates: Interaction of Esterases with Esters of Organophosphorus and Carbamic Acids. North-Holland, Amsterdam

26 Shafferman, A., Velan, B., Ordentlich, A., Kronman, C., Grosfeld, H., Leitner, M., Flashner, Y., Cohen, S., Barak, D. and Ariel, N. (1992) Substrate inhibition of acetylcholinesterase: residues involved in signal transduction from the surface to the catalytic center. EMBO J. **11**, 3561–3568

27 Malany, S., Sawai, M., Sikorski, R. S., Seravalli, J., Quinn, D. Q., Radić, Z., Taylor, P., Kronman, C., Velan, B. and Shafferman, A. (2000) Transition state structure and rate determination for the acylation stage of acetylcholinesterase catalyzed hydrolysis of (acetylthio)choline. J. Am. Chem. Soc. **122**, 2981–2987

28 Millard, C. B., Koellner, G., Ordentlich, A., Shafferman, A., Silman, I. and Sussman, J. L. (1999) Reaction products of acetylcholinesterase and VX reveal a mobile histidine in the catalytic triad. J. Am. Chem. Soc. **121**, 9883–9884

29 Millard, C. B., Kryger, G., Ordentlich, A., Greenblatt, H. M., Harel, M., Raves, M. L., Segall, Y., Barak, D., Shafferman, A., Silman, I. and Sussman, J. L. (1999) Crystal structures of aged phosphonylated acetylcholinesterase: nerve agent reaction products at the atomic level. Biochemistry **38**, 7032–7039

30 Changeux, J.-P. (1966) Responses of acetylcholinesterase from *Torpedo marmorata* to salts and curarizing drugs. Mol. Pharmacol. **2**, 369–392

31 Epstein, D. J., Berman, H. A. and Taylor, P. (1979) Ligand-induced conformational changes in acetylcholinesterase investigated with fluorescent phosphonates. Biochemistry **18**, 4749–4754

32 De Ferrari, G. V., Mallender, W. D., Inestrosa, N. C. and Rosenberry, T. L. (2001) Thioflavin T is a fluorescent probe of the acetylcholinesterase peripheral site that reveals conformational interactions between the peripheral and acylation sites. J. Biol. Chem. **276**, 23282–23287

33 Ordentlich, A., Barak, D., Kronman, C., Ariel, N., Segall, Y., Velan, B. and Shafferman, A. (1996) The architecture of human acetylcholinesterase active center probed by interactions with selected organophosphate inhibitors. J. Biol. Chem. **271**, 11953–11962

34 Wong, L., Radić, Z., Brüggemann, R. J. M., Hosea, N. A., Berman, H. A. and Taylor, P. (2000) Mechanism of oxime reactivation of acetylcholinesterase analyzed by chirality and mutagenesis. Biochemistry **39**, 5750–5757

35 Kaplan, D., Ordentlich, A., Barak, D., Ariel, N., Kronman, C., Velan, B. and Shafferman, A. (2001) Does "butyrylization" of acetylcholinesterase through substitution of the six divergent aromatic amino acids in the active center gorge generate an enzyme mimic of butyrylcholinesterase? Biochemistry **40**, 7433–7445